J. Aerosol Sci., Vol. 24, No. 2, pp. 237–253, 1993
Printed in Great Britain.

0021–8502/93 $6.00+0.00
Pergamon Press Ltd

SODIUM AEROSOL FORMATION AND REMOVAL MECHANISMS IN THE FAST REACTOR COVER GAS SPACE

I. J. FORD

Theoretical Studies Department, AEA Industrial Technology, B424.4, Harwell Laboratory, Didcot, Oxon OX11 0RA, U.K.

(*Received* 4 *June* 1992; *and in final form* 14 *September* 1992)

Abstract—The transport of sodium across the cover gas space onto structures on the roof of the reactor vessel can pose some problems in fast reactor design. Mechanisms for this include the condensation of vapour onto the cool surfaces, and the deposition of sodium aerosol by thermophoresis, diffusiophoresis and turbulent impaction. A model of cover gas thermal hydraulics and aerosol dynamics is described which includes these transport mechanisms and which can help in the interpretation of experiments on cover gas aerosol behaviour. It is found that a single parameter, related to the particle nucleation rate, can characterize a series of Japanese tests conducted with a variable sodium pool temperature but a constant roof temperature. Furthermore, at very low pool temperatures it appears that particle nucleation is not possible and that the system is dominated by an introduced aerosol.

NOMENCLATURE

a, b, c, d, e	coefficients in growth and removal equations
A	area
B	parameter in c_e
c_e	equilibrium vapour mass fraction
$\bar{c}_p$	density averaged specific heat capacity
Cn_s	surface condensation number
D	vapour diffusion coefficient
DS_r	droplet–roof view factor
DS_p	droplet–pool view factor
DS_w	droplet–wall view factor
F	quantity in size distribution
g	acceleration due to gravity
h_{gs}	pool-to-roof heat transfer coefficient
h_w	wall-to-cavity heat transfer coefficient
i	vapour flux
J	particle removal flux
k	gas thermal conductivity
k_B	Boltzmann's constant
$\langle k_e^* \rangle$	wavelength averaged extinction coefficient
$\langle k_a^* \rangle$	wavelength averaged absorption coefficient
K	coagulation kernel
L	sodium latent heat of evaporation
n	particle size distribution
p	pressure
q	heat flux
R	aerosol radius
R_0	nucleation radius
S	peak supersaturation in boundary layer
S_n	particle creation rate
S_pS_r	pool–roof view factor
S_wS_r	wall–roof view factor
t	time
T	temperature
u	e/a
v	particle removal velocity
v_0	liquid molecular volume
V	cavity volume
V_a	volume concentration of aerosol
w	d/a
x	c/a
y	b/a
ε	collision efficiency
ϕ_s	particle settling flux

η gas viscosity
λ mean free path
ω albedo of cavity mixture
ν exponent in size distribution
ρ density of cavity mixture
ρ_L sodium liquid density
ρ_{ve} equilibrium vapour density
σ Stefan–Boltzmann constant
σ_c collision diameter
τ_o optical thickness of cavity mixture

Suffices

ℓ surface label
p pool
r roof
w wall

Superscripts

g gravitational
T thermophoretic
TU turbulent

1. INTRODUCTION

The cover gas space of a pool-type fast reactor is an inert gas blanket lying between a hot pool of liquid sodium coolant and a relatively cold roof structure. The geometry is illustrated in Fig. 1, and can be likened to that of a diffusion chamber except that the temperature gradients are sufficient to drive a turbulent convective flow around the cavity. The cover gas space is designed to allow for coolant volume changes which take place when the operating temperature of the reactor varies. However, due to the large temperature gradients present, sodium evaporates into the cavity, where it can condense to form an aerosol. This can have an important effect on the heat transfer across the blanket and therefore on the operating conditions of the reactor. Furthermore, sodium can be transported across the cavity onto sensitive roof structures, such as penetrations which allow the insertion of control rods, which for reasons of safety must be kept free of solid sodium deposits. Vapour condensation onto a surface is driven by a temperature difference between the surface and vapour in the cavity, and there is also the possibility of aerosol deposition by various mechanisms, such as thermophoresis, diffusiophoresis and turbulent impaction. Theoretical modelling can be an important aid in understanding sodium transport in the cover gas and in optimizing a design.

The purpose of this paper is to describe the current state of development in cover gas aerosol modelling, and to present calculations to interpret a series of Japanese experiments investigating cover gas behaviour. Emphasis is given to the process of particle nucleation, which controls the aerosol density and determines whether the properties of the cavity are strongly or weakly affected by its presence. It turns out that the nucleation rate is undetermined by theory at present and is best represented as a free parameter which can be adjusted to fit experiment.

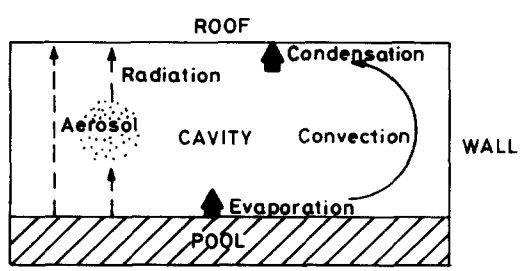

Fig. 1. Typical geometry of the fast reactor cover gas space.

2. THERMAL MODELLING

2.1. *Heat transfer*

There are two aspects to the modelling of the cover gas cavity: the analysis of heat transfers from the hot pool of molten sodium to the cool roof, with the possible involvement of walls and intervening aerosol; and the formation and removal processes which determine the amount of aerosol in the cavity. We shall briefly describe the thermal aspects in this section, including the important calculation of evaporation/condensation mass transfer rates at surfaces. A wider discussion of these aspects is to be found elsewhere (Sinai *et al.*, 1993).

We shall consider heat transfers into and across a simplified cylindrical cavity in the following to illustrate the modelling. The temperature T_b of the central well-mixed region of the cavity (and by assumption that of the aerosol) is determined by balancing the heat inputs and losses, which include radiative, convective and condensative mechanisms:

$$A_p(DS_p\sigma(T_p^4-T_b^4)+h_{gs}(\xi(T_p)-\xi(T_b)))+A_w(DS_w\sigma(T_w^4-T_b^4)+h_w(\xi(T_w)-\xi(T_b)))$$
$$=A_r(DS_r\sigma(T_b^4-T_r^4)+h_{gs}(\xi(T_b)-\xi(T_r))), \quad (1)$$

where A_p, A_r and A_w are the surface areas of the pool, roof and walls, respectively; DS_p, DS_r and DS_w the droplet to pool, roof and wall view factors associated with radiative heat transfer between surfaces according to Stefan's law. T_p, T_r and T_w are the pool, roof and wall absolute temperatures, σ the Stefan–Boltzmann constant, h_{gs} and h_w the pool-to-roof and wall-to-cavity heat transfer coefficients, and ξ, describing the joint convective and condensative heat transfers, is given by (Clement, 1985a)

$$\xi=T-\frac{L}{\bar{c}_p}\ln(1-c_e), \quad (2)$$

where L is the latent heat of condensation, $\bar{c}_p$ the density averaged specific heat capacity of the cavity mixture of argon and sodium vapour, and c_e is the equilibrium vapour mass fraction ($c_e=\rho_{ve}/\rho$ with ρ_{ve} the equilibrium vapour density and ρ the total density of the cavity mixture). The heat transfer coefficients are defined as

$$h_{gs}=h_{gs}^{\circ}k\left(\frac{g(T_p-T_r)}{T}\left(\frac{\rho^2\bar{c}_p}{k\eta}\right)\right)^{1/3} \quad (3)$$

$$h_w=h_w^{\circ}k\left(\frac{g|T_w-T_b|}{T}\left(\frac{\rho^2\bar{c}_p}{k\eta}\right)\right)^{1/3}, \quad (4)$$

where k and η are the thermal conductivity and viscosity of the cavity mixture, g is the acceleration due to gravity and h_{gs}° and h_w° are coefficients which for infinite surface areas are 0.15 and 0.13, respectively (McAdams, 1954). For horizontal plates separated by a small distance, which usually applies in the cover gas case, the convective heat transfer coefficient is arguably better described using an overall plate-to-plate correlation as given in equation (3), rather than separate pool–cavity and cavity–roof correlations involving (T_p-T_b) and (T_b-T_r), respectively, since the boundary layer processes at each plate cannot be considered to be decoupled unless the separation is large. The pool-to-roof convective heat transfer for this situation in the absence of condensation is

$$q=h'_{gs}(T_p-T_r), \quad (5)$$

with h'_{gs} given by equation (3) with $h_{gs}^{\circ}=0.075$ (McAdams, 1954). We have assumed that the boundary layer heat transfers are characterized by equal heat transfer coefficients, so

$$q=h_{gs}(T_p-T_b)=h_{gs}(T_b-T_r) \quad (6)$$

in the absence of an aerosol. With the assumption that $(T_b-T_r\approx(T_p-T_r)/2$ we obtain a value of h_{gs}° in equation (3) equal to 0.15. The inclusion of condensative transfers then leads to the $h_{gs}\Delta\xi$ terms in equation (1). The differences between such a treatment and one based on separate correlations for the pool and roof boundary layers are not expected to be great.

The total heat transfer to the roof is written

$$q_{TOT} = q_r + S_p S_r \sigma(T_p^4 - T_r^4) + DS_r \sigma(T_b^4 - T_r^4) + S_w S_r \sigma(T_w^4 - T_r^4), \tag{7}$$

where q_r is the convective–condensative component:

$$q_r = h_{gs}(\xi(T_b) - \xi(T_r)) \tag{8}$$

and $S_p S_r$ and $S_w S_r$ the pool- and wall-to-roof radiative view factors.

The radiative transfer view factors are calculated according to the optical depth τ_o and scattering albedo ω of the cavity mixture. These parameters are determined by the aerosol size distribution and the size-dependent absorption and scattering efficiencies, which are discussed below. The pool and roof view factors with respect to each other and with the cavity are calculated using one-dimensional infinite plate formulae due to Williams (1983, 1984). In this paper, view factors between the wall and either pool or roof are ignored and the wall-to-bulk view factor is set to be its value at infinite τ_o, thus simplifying the necessary analysis and overcoming difficulties of geometry. As wall heat transfers are usually small, this is probably an adequate approximation. Radiative heat transfers make an important contribution to the total heat fluxes in the system, though for typical sodium and roof temperatures, convective heat transfers are larger. The condensative heat transfers usually make the smallest contributions.

2.2. *Mass transfer*

The rate of evaporative/condensative mass transfer at each surface is related to the associated convective–condensative heat transfer. This quantity has been already defined as q_r for the roof and now we introduce analogous quantities q_p and q_w for the pool and walls, respectively. The parameter which determines the relationship is the surface condensation number Cn_s (Clement, 1985a). The mass transfer rate at each surface is written

$$i_\ell = \frac{q_\ell}{L(1 + Cn_s(T_\ell, S_\ell))}, \tag{9}$$

where ℓ denotes p, r or w and Cn_s is a function of the surface temperature T_ℓ and the peak supersaturation S_ℓ in the adjacent boundary layer. This supersaturation is determined by the amount of aerosol in the boundary layer and ranges from unity, when copious quantities of aerosol are present, to a maximum S_ℓ^{max} when no aerosol is present. The relationship between S_ℓ and aerosol properties will be discussed shortly.

The extremes of aerosol density lead to bounds on the values of Cn_s. For a dense aerosol, $S_\ell = 1$ and

$$Cn_s(T_\ell, S_\ell = 1) = \frac{k(1 - c_e)}{LD\rho c_e'}, \tag{10}$$

where c_e' is the derivative of c_e with respect to temperature, and D is the vapour diffusion coefficient. All quantities are evaluated at the surface temperature T_ℓ. For no aerosol, $S_\ell = S_\ell^{max}$ and

$$Cn_s(T_\ell, S_\ell^{max}) = \frac{Cn_s(T_\ell, S_\ell = 1)c_e'}{(1 - c_e)\Delta \ln(1 - c_e)/(T_b - T_\ell)}, \tag{11}$$

where $\Delta \ln(1 - c_e) = \ln(1 - c_e(T_\ell)) - \ln(1 - c_e(T_b))$. This bound can be greater or smaller than $Cn_s(T_\ell, S_\ell = 1)$ depending on whether T_ℓ is greater or smaller than T_b. S_ℓ^{max} is defined by

$$S_\ell^{max} = \frac{c_e(T_b)(T_m - T_\ell) - c_e(T_\ell)(T_m - T_b)}{c_e(T_m)(T_b - T_\ell)} \tag{12}$$

with T_m given by

$$T_m = \frac{B}{2}\left(1 - \left(1 - \frac{4}{B}\left[\frac{c_e(T_b)\,T_\ell - c_e(T_\ell)\,T_b}{c_e(T_b) - c_e(T_\ell)}\right]\right)^{1/2}\right), \tag{13}$$

with $c_e \propto \exp(-B/T)$ defining the parameter B.

For values of S_ℓ between 1 and $S_\ell^{\max}$, the calculation of Cn_s is more complicated:

$$Cn_s(T_\ell, S_\ell) = \frac{Cn_s(T_\ell, S_\ell = 1)c'_e}{(1-c_e(T_\ell))\ln\left(\dfrac{1-c_e(T_\ell)}{1-S_\ell c_e(T_N)}\right)\Big/(T_N - T_\ell)}, \tag{14}$$

with T_N, the temperature in the boundary layer at which the supersaturation reaches its peak, given by

$$c'_e(T_N)S_\ell = \frac{S_\ell c_e(T_N)-1}{T_N - T_\ell}\ln\left(\frac{1-c_e(T_N)S_\ell}{1-c_e(T_\ell)}\right). \tag{15}$$

As $S_\ell \to S_\ell^{\max}$, $T_N \to T_m$. For S_ℓ close to 1, this formalism yields an approximation used previously (Clement, 1985b):

$$Cn_s(T_\ell, S_\ell \approx 1) = \frac{Cn_s(T_\ell, S_\ell = 1)}{1 \pm (S_\ell - 1)^{1/2}(c_e c''_e)^{1/2}/c'_e}, \tag{16}$$

with the sign depending on that of $(T_b - T_\ell)$. Equation (14), however, is more appropriate and leads to the correct limit as $S_\ell^{\max}$.

2.3. *Aerosol coupling to thermal modelling*

Finally, we discuss the relationship between S_ℓ and aerosol properties, which provides the link between the thermal and aerosol aspects of the modelling problem. A simple model of vapour diffusion across a stagnant boundary layer in the presence of an aerosol which acts as a local vapour sink (by condensation onto the aerosol) yields a vapour concentration profile from which a maximum supersaturation can be calculated (Clement, 1987). The resulting relationship between S_ℓ and the aerosol properties can be written

$$S_\ell - 1 = \left(\frac{dT}{dx}\right)^2 \frac{c''_e(T_\ell)}{c_e(T_\ell)} \frac{1}{4\pi N \bar{R}}(1 - \operatorname{sech}\phi), \tag{17}$$

where dT/dx is the temperature gradient at the surface, N is the aerosol number density in the boundary layer, $\bar{R}$ its mean radius, and

$$\phi = (\pi N \bar{R} \delta^2)^{1/2} \tag{18}$$

with δ a length scale which can be related to $S_\ell^{\max}$:

$$\delta^2 = \frac{8c_e(T_\ell)}{\left(\dfrac{dT}{dx}\right)^2 c''_e(T_\ell)}(S_\ell^{\max} - 1). \tag{19}$$

This expression for S_ℓ incorporates the correct behaviour for the dense aerosol limit ($N\bar{R} \to \infty$), and the no-aerosol limit ($N\bar{R} \to 0$). These are, respectively, equation (17) without the $\operatorname{sech}\phi$ term, and

$$S_\ell = (S_\ell^{\max} - 1)\left(1 - \frac{5\pi}{12} N \bar{R} \delta^2\right) + 1. \tag{20}$$

The full expression, equation (17) provides an interpolation between the two. The temperature gradient at each surface is evaluated using

$$\left(\frac{dT}{dx}\right) = \frac{q_\ell}{k(1 + 1/Cn_s(T_\ell, S_\ell))}. \tag{21}$$

It is assumed that the aerosol density is constant throughout the cavity, including the boundary layers, so that equation (17) provides a link between the supersaturations at each surface. This is not necessarily so, since aerosol may fail to penetrate close enough to downward facing surfaces. However, we shall ignore this possibility here.

The modelling of mass transfers in the cavity is treated, therefore, by assuming a peak supersaturation one surface, from which the condensation numbers at each surface may be found, and with the help of the thermal analysis, which requires the optical parameters τ_0 and ω but is only slightly affected by the condensation numbers and hence the degree of aerosol coupling, the mass transfer rates by evaporation and condensation may be calculated. The net evaporation rate into the cavity is given by

$$Ai_d = \frac{A_p q_p}{L(T_p)(1+Cn_s(T_p, S_p))} + \frac{A_w q_w}{L(T_w)(1+Cn_s(T_w, S_w))} - \frac{A_r q_r}{L(T_r)(1+Cn_s(T_r, S_r))}, \quad (22)$$

with suitable neglect of the wall term if the wall is hotter than the bulk but not a wet surface. The quantity i_d is an effective mass flux across all surfaces facing the cavity, with total surface area A. This net evaporative mass input into the cavity condenses onto the aerosol and is then equal to the total aerosol loss rate, in a steady state. It is the source term which, together with models for aerosol removal, will be used in the next section to determine the aerosol distribution.

3. AEROSOL ANALYSIS

The aerosol size distribution $n(R)$ averaged over the cavity (the number of particles in the size range R to $R+\mathrm{d}R$ per unit volume) evolves according to the following equation:

$$\frac{\partial n}{\partial t} + \sum_{\ell} \frac{J_\ell(R)}{V} + \frac{\partial}{\partial R}(\dot{R}n) - S_n - Kn^2 = 0, \quad (23)$$

where $J_\ell(R)$ is the removal current of radius R droplets at surface ℓ, $\dot{R}$ the single droplet growth rate, S_n the particle creation rate and Kn^2 the coagulation terms, which are written

$$Kn^2 = \frac{1}{2}\int \mathrm{d}R_1\,\mathrm{d}R_2\,\delta[R-(R_1^3+R_2^3)^{1/3}]\,K(R_1, R_2)n(R_1)n(R_2)$$

$$-\int \mathrm{d}R_1\,K(R_1, R)n(R_1)n(R), \quad (24)$$

with $K(R_1, R_2)$ the coagulation kernel representing the rate of coalescence of droplets of radii R_1 and R_2. We shall drop Kn^2 from equation (23) but an estimate of its size and importance will be made later. Equation (23) describes the aerosol in the well mixed central region of the cavity, hence the averaging over volume. The particle creation and removal rates are taken to apply as fluxes at the boundary.

3.1. *Growth*

The growth rate $\dot{R}$ is known as a function of R and is taken to consist of a condensation term and a radiative redistribution term (Barrett and Clement, 1990):

$$\dot{R} = \frac{a}{R} + b \quad (25)$$

where

$$a = \frac{1}{4\pi\rho_L VN\bar{R}}\left(Ai_d - \frac{A_p q_p + A_w q_w - A_r q_r}{L(1+Cn)}\right) \quad (26)$$

$$b = \frac{A_p q_p + A_w q_w - A_r q_r}{4\pi\rho_L(1+Cn)VN\overline{R^2}} \quad (27)$$

with Cn given by equation (10) evaluated at T_b, and ρ_L the density of liquid sodium. The first term in equation (25) describes condensation on particles in the μm region, the size range of most importance in the following. The parameter b and the second term in

equation (26) result from a possible net radiative heat loss from the aerosol. The second term is less important than the condensative term. Additional redistributive terms could be added, such as Ostwald ripening (Lifshitz and Slyozov, 1961). However, redistributive terms act over long timescales (Barrett *et al.*, 1992) and since the lifetime of a sodium droplet in the cavity is relatively short, they have only a slight effect on the cover gas aerosol.

In order to calculate the steady state size distribution and hence all the properties of the aerosol, we need to solve the first order differential equation, equation (23), setting $\partial n/\partial t = 0$. This is made easier if we assume that the aerosol removal velocities v_ℓ can be expressed as a power series in R since we can then make analytic progress. This is particularly convenient since to a first approximation the removal velocities according to several mechanisms can be expressed as powers of R.

3.2. *Particle removal*

The removal currents can be written

$$J_\ell(R) = A_\ell v_\ell n, \tag{28}$$

where A_ℓ is the surface area and v_ℓ the removal velocity, at radius R, onto surface ℓ. We consider gravitational settling:

$$v_\ell^{\mathrm{g}} = \frac{2\rho_{\mathrm{L}} g}{9\eta} R^2, \tag{29}$$

thermophoretic removal (expression applicable for $R \geq 1\ \mu\mathrm{m}$ and for a very high ratio of particle to gas thermal conductivities (Talbot *et al.*, 1980)):

$$v_\ell^{\mathrm{T}} = 1.328 \frac{\lambda}{R} \frac{k}{p} \nabla T, \tag{30}$$

and diffusiophoresis:

$$v_\ell^{\mathrm{d}} = \frac{p_{\mathrm{ve}} i_\ell}{\left[\left(\frac{m_{\mathrm{g}}}{m_{\mathrm{v}}}\right)^{1/2} (p - p_{\mathrm{ve}}) + p_{\mathrm{ve}}\right] \rho_{\mathrm{ve}}}, \tag{31}$$

where ρ_{L} is the condensate density, η the gas viscosity, λ the gas phase mean free path ($\lambda = k_{\mathrm{B}} T/(\sqrt{2}\pi p \sigma_{\mathrm{c}}^2)$ with σ_{c} the collision diameter) p the pressure, ∇T the temperature gradient at the surface, m_{g} the inert gas molecular mass, m_{v} the vapour molecular mass and p_{ve} the equilibrium vapour pressure. Gravitational removal usually dominates for typical conditions: thermophoresis and diffusiophoresis make smaller contributions depending on the particle size. Particle removal onto downward facing surfaces, of course, does not contain a gravitational element.

We also consider the mechanisms of turbulent impaction, but since no model for impaction from a convective flow appears to be available, we assume the deposition velocity is a constant, v_ℓ^{TU}, and treat it as an input parameter. It is not likely to be an important removal mechanism.

3.3. *Particle creation*

The creation rate S_{n} is a function of size. For later use it will be convenient to consider the particle creation to occur at two sizes: R_{o} and R_{n}. The first represents nucleation of new particles at nm sizes (by a homogeneous or heterogeneous process). The particle creation rate at size R_{n} will represent an injection rate of aerosol particles by a process other than nucleation and R_{n} will be taken to be in the μm range. S_{n} is written

$$S_{\mathrm{n}}(R) = S_{\mathrm{no}}^{\mathrm{NUC}} \delta(R - R_{\mathrm{o}}) + S_{\mathrm{no}} \delta(R - R_{\mathrm{n}}). \tag{32}$$

The total nucleation plus injection rate per unit volume is then $S_{\mathrm{no}}^{\mathrm{NUC}} + S_{\mathrm{no}}$.

3.4. *Size distributions*

If we write $\Sigma J_\ell / V = jn$ then from equation (23) we have, using equation (25)

$$\left(\frac{a}{R}+b\right)\frac{\partial n}{\partial R}+\left(j-\frac{1}{R^2}\right)n=-S_n(R) \tag{33}$$

which, using equation (32) for S_n, gives

$$n(R)=\frac{S_{no}^{NUC}}{a/R_o+b}\exp[(G(R)-G(R_o))]+\frac{S_{no}}{a/R_n+b}\exp[(G(R)-G(R_n))] \tag{34}$$

for $R>R_n$. For $R<R_n$, the injected particle radius, the second term in equation (34) does not appear. The exponent function G is given by

$$G(R)=\int\left(\frac{a/R^2+j}{a/R+b}\right)dR. \tag{35}$$

This can be evaluated, and hence the size distribution found, if j is expressed as a series of powers of R. As an example, consider the case of no radiative redistribution ($b=0$), no injected aerosol ($S_{no}=0$) and removal only by gravitational settling ($j=A_p v_p^g/V$): the solution is

$$n(R)=\frac{S_{no}^{NUC}R}{a}\exp[-\alpha(R^4-R_0^4)], \tag{36}$$

where

$$\alpha=\frac{2\pi\rho_L^2 A_p g N\bar{R}}{9\eta\, A i_d}. \tag{37}$$

In practice, $\alpha R_0^4 \ll 1$ and so, writing $S_{no}^{NUC}=n_o a$, where n_o is a constant, we obtain $n(R)=n_o R\exp(-\alpha R^4)$, a size distribution used previously (Clement, 1985b).

If we write, in a general case, but still ignoring particle injection,

$$j=\sum_\ell (c_\ell R^2-d_\ell-e_\ell/R), \tag{38}$$

which includes all the R dependences described in equations (29–31), then we have

$$n(R)=\frac{n_o R}{1+yR}\exp(v_p+v_r+v_w), \tag{39}$$

where $y=b/a$. The factors v_ℓ are given by

$$v_\ell(R)=\int\frac{(x_\ell R^3-w_\ell R-u_\ell)\,dR}{1+yR}, \tag{40}$$

with $x_\ell=c_\ell/a$, $w_\ell=d_\ell/a$ and $u_\ell=e_\ell/a$. Where the gravitational velocity opposes the thermophoretic and diffusiophoretic velocities, the total removal velocity will be zero over a particular size range. This is the case for the pool and roof surfaces, where removal does not occur below a size R_{min} and above a size R_{max}, respectively. The opposition of the removal velocities is reflected in the sign convention chosen in equation (38). At vertical surfaces, no such considerations need be made.

The sizes R_{min} and R_{max} are found by solving the following equations:

$$x_p R_{min}^3-w_p R-u_p=0, \tag{41}$$

$$x_r R_{max}^3-w_r R-u_r=0. \tag{42}$$

We finally obtain

$$v_p=\begin{cases}F_p(R)-F_p(R_{min}), & R>R_{min}\\ 0, & R<R_{min}\end{cases} \tag{43}$$

$$v_r = \begin{cases} 0, & R > R_{max} \\ F_r(R) - F_r(R_{max}), & R < R_{max} \end{cases} \tag{44}$$

$$v_w = F_w(R), \tag{45}$$

with

$$F_p(R) = \frac{-x_p}{y^4}(yR - \tfrac{1}{2}(yR)^2 + \tfrac{1}{3}(yR)^3 - \ln(1+yR)) + \frac{w_p}{y^2}(yR - \ln(1+yR)) + \frac{u_p}{y}\ln(1+yR) \tag{46}$$

and $F_r(R)$ of the same form with x_p, w_p, u_p replaced by x_r, w_r, u_r and similarly for $F_w(R)$ with the x_p term ignored and w_p, u_p replaced by w_w, u_w. In all expressions the nucleation radius R_o has been ignored since it is very much smaller than the size range of interest.

The inclusion of particle injection at a radius R_n is very simple and consists of the multiplication of equation (39) by a factor for R greater than R_n, i.e. from equation (34) we obtain

$$n(R) = \frac{n_o R}{1+yR}\exp(v_p + v_r + v_w)\left[1 + \frac{S_{no}}{S_{no}^{NUC}\exp(v_p(R_n) + v_r(R_n) + v_w(R_n))}\right] \tag{47}$$

for $R > R_n$. If we again consider the simple case where gravitational settling dominates aerosol removal, and radiative redistribution is ignored, but include the injection of particles of radius R_n then the size distribution is

$$n(R) = \begin{cases} n_o R\exp(-\alpha R^4), & R < R_n \\ n_o R\exp(-\alpha R^4)\left[1 + \dfrac{S_{no}}{S_{no}^{NUC}}\exp(\alpha R_n^4)\right], & R > R_n \end{cases} \tag{48}$$

The size distribution provides the key to the aerosol modelling, since from it the aerosol density ρ_a, mean radius, etc. can be found. The optical properties of the aerosol are found from the following:

$$\tau_o = \frac{\langle k_e^* \rangle}{V_a}\frac{10^6 \rho_a d}{\rho_L} \tag{49}$$

$$\omega = 1 - \frac{\langle k_a^* \rangle}{\langle k_e^* \rangle}, \tag{50}$$

where $\langle k_e^* \rangle$ and $\langle k_a^* \rangle$ are the wavelength averaged extinction and absorption coefficients, V_a is the volume concentration of the aerosol and d the height of the cavity (Barrett and Clement, 1985). The combination $\langle k_e^* \rangle / V_a$ in equation (49) is in units of $m^{-1}/cm^3 m^{-3}$. Using preliminary Mie calculations to set up a database of optical properties at various temperatures for a range of sizes, the optical parameters of the actual size distribution given by equation (47), can be calculated.

4. THE SOLUTION ALGORITHM AND PARTICLE NUCLEATION

The cover gas thermal hydraulic and aerosol modelling problems have now ben formulated and the links between them specified. It is most convenient to solve the combined problem in an iterative manner. Assuming certain values of the optical parameters τ_o and ω, the thermal sector of the model can be solved, giving temperatures and heat transfer rates. If, in addition, the supersaturation in a single boundary layer is chosen, then this determines the evaporation/condensative fluxes at all surfaces, and the aerosol parameter combination $N\bar{R}$. With this, and an approximate value of the second moment of the size distribution, $N\overline{R^2}$, the growth parameters a and b are specified, and in the absence of particle injection, this determines the constant n_o in the size distribution. An iterative procedure is then used to obtain a consistent value of $N\overline{R^2}$. If particle injection does take place, then the injection rate

S_{no} and radius R_n are also required, together with an initial estimate of n_o. Another procedure of iteration produces a consistent value of n_o. Once n_o is known, the optical properties of the aerosol are calculated and the whole process repeated, starting with the thermal-hydraulic problem. Only a few iterations are needed to produce a consistent solution for the whole system, and then predictions are made for the heat transfers, mass transfers and aerosol density and mean size.

The one unknown parameter is the peak supersaturation in the chosen boundary layer. In fact, if the assumption of constant aerosol density throughout the cavity fails, then this quantity needs to be chosen in more than one boundary layer. For instance, the aerosol in the roof boundary layer may be less dense than elsewhere in the cavity, due to gravitational settling. However, we assume here that the density is constant throughout and so only one boundary layer supersaturation need be specified.

The peak supersaturation is determined by the rate of particle nucleation in the boundary layer. However, this sector of the model remains undetermined. Nucleation occurs either by a homogeneous or heterogeneous mechanism, where the nm size condensation nuclei consist of clusters of vapour molecules or foreign particles, respectively. Both require a degree of supersaturation, which limits the formation to boundary layers, and if foreign nuclei are present, then heterogeneous nucleation generally occurs at lower supersaturations than the homogeneous process.

If the formation mechanism is heterogeneous, the supersaturation at which foreign particles of radius R_o become condensation nuclei is

$$S_c = \ln\left(\frac{2\sigma v_o}{R_o k_B T}\right), \tag{51}$$

where σ is the surface tension of sodium, v_o the liquid volume per molecule and k_B Boltzmann's constant. The critical supersaturation, for a given R_o, is lowest for the pool boundary layer, but since the boundary layer supersaturation behaves like $c'_e/c_e \propto 1/T^2$, the roof boundary layer has the largest supersaturation. Nucleation is therefore likely to occur close to the roof. If condensation nuclei are available, then the nucleation rate will depend on the rate of supply of foreign particles to the boundary layer, and the growth rate of the nuclei, which will be a function of supersaturation. The heterogeneous nucleation rate will be an increasing function of supersaturation, with a threshold given by equation (51), below which nucleation does not occur.

Homogeneous nucleation would occur if foreign particles are systematically removed from the system. With every heterogeneously nucleated droplet that is removed, a foreign particle is lost, and so for heterogeneous nucleation to continue, a supply of foreign particles is needed. If the cover gas is continuously replenished, then such particles may be provided, but if the system is closed, and remains so for a period of time, and if no foreign particles are generated internally, then the supply of heterogeneous nuclei will be exhausted and homogeneous nucleation will take over.

Homogeneous nucleation is not well described theoretically at present, and the most that can be said is that the rate increases rapidly with temperature and supersaturation. There is an apparent threshold supersaturation, due to the great sensitivity. In both nucleation processes, fluctuations in supersaturation in the boundary layers will have an important effect, adding to the difficulty in modelling particle formation.

The total rate of nucleation is shown schematically in Fig. 2, as a function of supersaturation S_ℓ. In a steady state, the rate of formation is equal to the rate of droplet removal, which is proportional to $N\overline{R^2}$ if dominated by gravitational settling. This quantity falls with supersaturation and vanishes at S_ℓ^{max}. The intersection of formation rate and removal rate curves, sketched in Fig. 2, determines the boundary layer supersaturation which characterizes the model.

Clearly, the ease with which nucleation occurs controls the state of the cover gas system. If heterogeneous nuclei are made available at a larger size, such that S_ℓ is reduced, or in greater quantities, which would enhance the heterogeneous nucleation rate, then the system

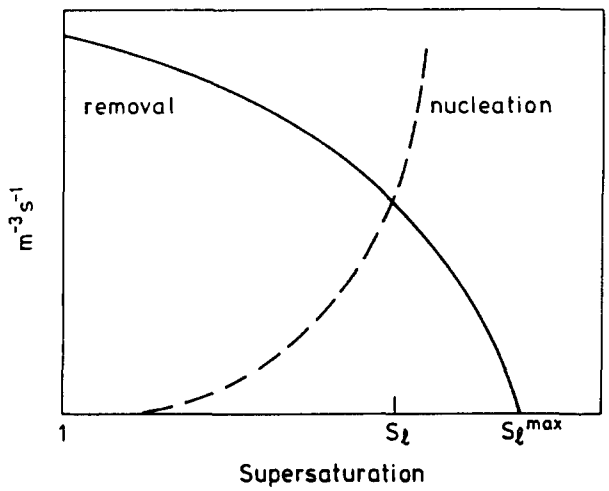

Fig. 2. Dependence of particle nucleation and removal rates on boundary layer supersaturation.

is driven to low supersaturations, and a dense aerosol. If, however, heterogeneous nuclei are absent and the homogeneous nucleation rate low the system is driven towards the thin aerosol limit, with high supersaturations. It would, in principle, be possible to change the state of the cover gas space by altering the supply of foreign particles, possibly by careful design of the cover gas replenishment system.

5. THE HIMENO–TAKAHASHI EXPERIMENTS

5.1. *Experiments*

The preceding discussion, and development of the modelling to incorporate particle injection, is aimed at interpreting a series of cover gas experiments performed by Himeno and Takahashi (1980). A sketch of the vessel used is given in Fig. 3. The only serious drawback, as regards ease of analysis, in the design of the experiment is the large ratio of wall to pool areas. However, the walls were well insulated and so their effect on the temperature of the cavity mixture, and the aerosol, may have been small. Argon of greater than 99.99% purity was passed continuously through the vessel at a low replenishment rate of 2–6 l min^{-1}. The cover gas volume was about 100 l. Laser light scattering, calibrated using filters on the argon outlet pipe, was used to measure the aerosol density ρ_a, and the aerosol settling flux ϕ_s in the centre of the cavity was determined using upward facing collection plates exposed in the cavity for a certain period.

Measurements of these two quantities were made for a roof temperature of 120°C and pool temperatures in a range from about 280 to 530°C. The data are shown in Fig. 4 against pool temperature. The aerosol density ranges from about 20 g m^{-3} at the highest pool temperature down to very low values of the order of 0.1 g m^{-3} at the lowest temperatures. Although error estimates were not provided, certain features in the data seem to emerge. Above about 350°C the settling rate and density rise with pool temperature; the settling rate with a reasonably constant slope but the aerosol density rising more steeply at first and then less so above about 420°C. Below 350°C the data are to an approximation independent of pool temperature. A partial explanation for these trends was proposed (Clement, unpublished work) involving the increasing importance of coagulation above 420°C, where the aerosol number density is large. The change in behaviour at 350°C, however, was not accounted for.

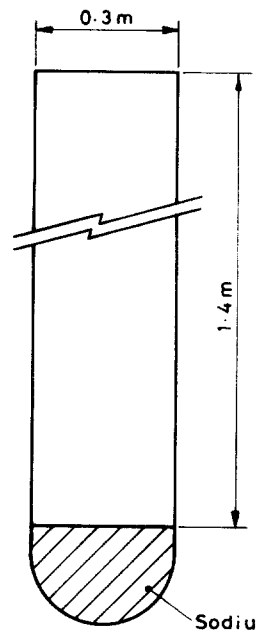

Fig. 3. Vessel used in the Himeno–Takahashi experiments.

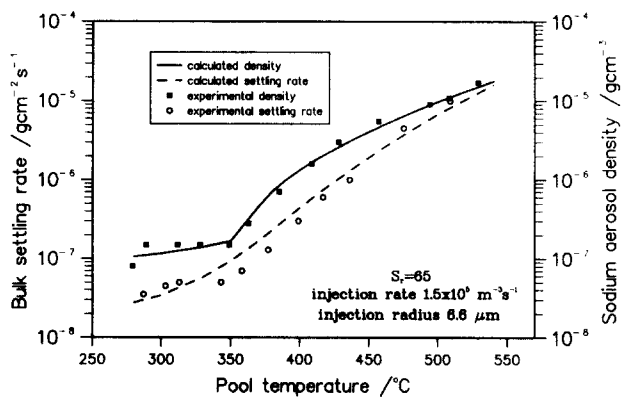

Fig. 4. Dependence of aerosol density and settling rate upon sodium pool temperature in the Himeno–Takahashi experiments.

5.2. *Estimate of coagulation*

The model described above does not include the effects of coagulation on the size distribution, but an estimate can be made of its importance. The dominant coagulation mechanism is likely to be differential gravitational settling, for which the kernel $K(R_1, R_2)$ in equation (24) is

$$K(R_1, R_2)=\pi(R_1+R_2)^2\frac{2\rho_L g}{9\eta}|R_1^2-R_2^2|\varepsilon(R_1, R_2), \tag{52}$$

where ε is the collision efficiency given, for example, by

$$\varepsilon(R_1, R_2)=1+\frac{1+p^2}{2(1+p)^3}-\frac{3}{2(1+p)}, \tag{53}$$

with p the smaller of the ratios R_1/R_2 and R_2/R_1 (Williams, 1988).

Integrating equation (23) over R, the ratio of the coagulation to the removal term is

$$f_c = \frac{\frac{1}{2}\int dR_1 dR_2 K(R_1, R_2) n(R_1) n(R_2)}{\sum \frac{A_\ell}{V} \int dR v_\ell(R) n(R)}, \tag{54}$$

and this can be evaluated using the calculated size distribution, assuming no coagulation. At 420°C, the ratio is 0.125, according to calculations to be described shortly, rising to 0.6 at the highest temperatures in the experimental range. These estimates of the importance of coagulation suggest that it does not play a major role, particularly in explaining the apparent change in behaviour at 420°C. Perhaps at the highest pool temperatures coagulation ought to be taken into account in the modelling, but for most of the temperature range its neglect is probably adequate.

5.3. *Calculations with constant* S_r

Calculations have been performed for a roof temperature of 120°C and a range of pool temperatures. The walls were ignored, the pool emissivity was taken to be that of liquid sodium (Barnett *et al.*, 1985), and the roof emissivity was 0.2. Turbulent impaction was ignored.

Consider a situation where the increase in the nucleation rate with supersaturation, shown in Fig. 2, is rapid above a threshold at S_T, so that S_T may be taken to be a good approximation to the supersaturation where the rates of nucleation and removal are equal, and hence the supersaturation which determines the rest of the model. S_T is temperature dependent, but for a constant T_r, the temperature T_N in the roof boundary layer at which the supersaturation reaches its peak is insensitive to the cavity temperature. Thus the threshold temperature is reasonably independent of pool temperature, and according to the above assumptions, results for a range of T_p ought to be correlated using a single roof supersaturation.

The curves shown in Fig. 4 support this idea since a good fit to the data is obtained using $S_r = 65$. For T_p greater than 350°C the observed behaviour of both settling rate and aerosol density is well described, and the "transition" temperature of 420°C naturally accounted for. The steep fall in ρ_a as the temperature decreases to 350°C is explained by the behaviour of S_r^{max}, the maximum value of S_r, as a function of T_p, shown in Fig. 5. As the temperature difference across the roof boundary layer increases, so does the maximum available supersaturation. Only above about 350°C is it possible to generate a high enough supersaturation to exceed the threshold. In the absence of other particle formation mechanisms (such as particle injection) the aerosol density would therefore vanish at 350°C, and the steep rise immediately above this temperature, and the apparent change in behaviour at 420°C, appear as a consequence.

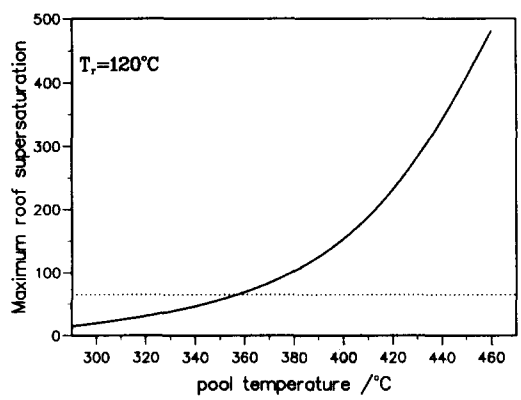

Fig. 5. Dependence of maximum roof supersaturation on pool temperature, with a threshold at 350°C for nucleation characterized by $S_r = 65$.

5.4. *Aerosol injection*

The residual aerosol observed below 350°C cannot therefore be formed by a nucleation mechanism, but more likely by the injection of particles. This possibility is supported by the behaviour of the settling rate, which levels off at the lowest pool temperatures. If net evaporation from the available surfaces were the only mass input into the cavity, then the settling rate, which in equilibrium is equal to the input rate, would continue to fall as the pool temperature is reduced. The fact that it remains approximately constant below 350°C suggests that there is an additional mass input to the cavity. Characterizing this input rate as the injection of 1.5×10^5 particles per unit volume per second, with a radius of 6.6 μm, and using the particle injection formalism outlined earlier, predictions of ρ_a and ϕ_s can be made for $T_p < 350$°C which account well for the data, and which are shown in Fig. 4. The calculations for $T_p > 350$°C also take account of this injection rate, but the effect of this inclusion is small, since the nucleation rate is much larger for these conditions, and the net evaporative mass input dominates.

The source for the particle injection is not perfectly clear, but there are at least two possibilities. Firstly, particles may be introduced along with the fresh argon which replenishes the cavity. However, it would seem unlikely such large particles could pass through the argon cleaning system, even at the assumed low concentration. Secondly, the particles could be created in the cavity by chemical reactions. Oxygen in the argon could react to form Na_2O, or hydrogen generated in the sodium pool by the reactions

$$2Na + NaOH = NaH + Na_2O$$

$$2NaH = 2Na + H_2$$

may enter the cavity and there form NaH. It was pointed out by Himeno and Takahashi (1980) that the formation of H_2 by the above reactions occurred in the temperature range $300°C < T < 380°C$. If all the NaOH in the pool gives rise to NaH in the cover gas, then it can be shown that 1 ppm by weight of NaOH in the pool gives about 0.13 gm^{-3} of NaH aerosol, for a pool depth of 0.4 m and a cavity height of 1.4 m. This mechanism has the additional feature that the aerosol density and settling rate fall again below 300°C, as seen experimentally.

The formation of such large particles purely from impurities in the sodium/argon system does seem unlikely, however, and it is worth considering other options. However, the options are few, assuming the data to be correct. The natural state of the system below the aerosol nucleation threshold is the totally decoupled state, with the vapour in the well-mixed region of the cavity having a density close to the mean of the equilibrium densities at roof and pool, with consequently a supersaturation in the bulk. The net evaporation rate i_d into the cavity tends to zero in this limit: the calculated evaporative input rate in the model, which assumes saturation in the bulk, is therefore an upper limit. This means that the calculated settling rate is also an upper limit. Considering a supersaturated cavity does not therefore help to explain the high values of ϕ_s at low temperatures, unless the collection plates measured not only the settling flux ϕ_s but also a condensation rate. This is possible since the cavity is supersaturated. However, the laser measurements indicate that an aerosol is present and so this line of reasoning does not seem to lead to an alternative explanation of the data. It is possible, however, that the laser scattering method for measuring aerosol concentrations was in error at low densities, since it appears to have been calibrated against filter measurements only down to a density of about 1 gm^{-3}.

5.5. *Discussion*

It is challenging to offer explanations for the cavity aerosol behaviour at low pool temperatures, but the more important results of these calculations apply to the higher temperatures. Using the roof supersaturation as the single free parameter, the data over a range of temperatures have been well accounted for. This is possible since the roof temperature is a constant, and it has been assumed that the roof supersaturation is at

a threshold value for particle nucleation, characteristic of this temperature. For different roof temperatures, the threshold supersaturation would change and it remains to be seen whether the insights gained from this experiment can be extended to other rigs.

It was suggested earlier that aerosol may fail to penetrate into the roof boundary layer due to gravitational settling, and that this boundary layer is therefore decoupled from the system and remains unsaturated. To illustrate this, Fig. 6 shows the size distribution calculated for the Himeno–Takahashi test with a pool temperature of 520°C. The maximum size particle which can be transported to the roof, by phoretic motion against the effect of gravitational settling, is about 4 μm. Assuming the roof boundary layer aerosol is limited in this way, the value of $N\bar{R}$ for the roof can be estimated to be only about 5–10% of the bulk value, suggesting the roof boundary is more supersaturated than might be thought, given a bulk value of $N\bar{R}$. This has been ignored here. If this were the case, then the pool supersaturation ought perhaps to be used as a more appropriate free parameter, and chosen to characterise the data instead of S_r. However, as it is likely that nucleation occurs at the roof, and it is therefore S_r which is more closely linked to the nucleation rate, such a treatment would be merely empirical.

Finally, the nature of the nucleation process can be speculated upon with the aid of Fig. 7. The supersaturation thresholds for heterogeneous nucleation, using equation (51) based on

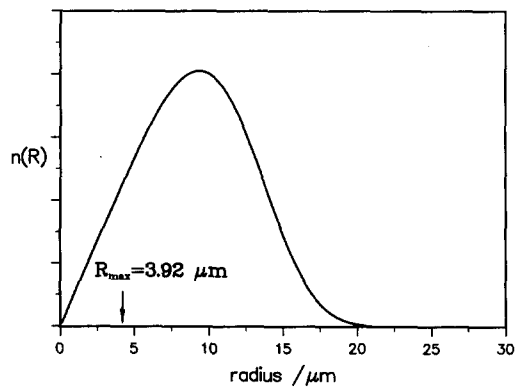

Fig. 6. Size distribution for a pool temperature of 520°C, compared with the maximum size that can penetrate to the roof, R_{max}.

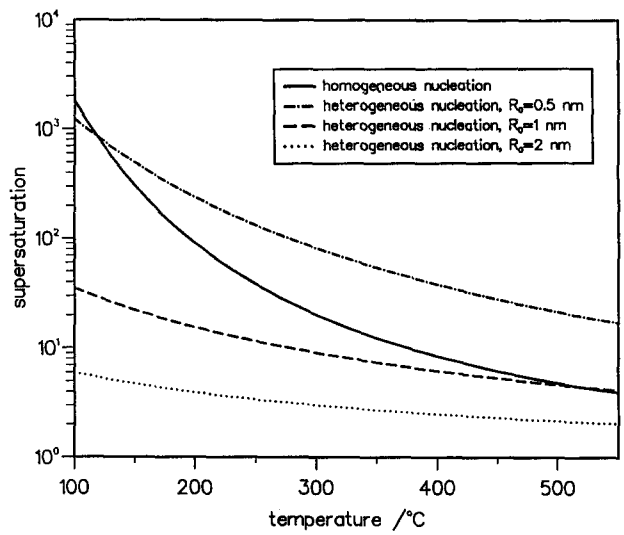

Fig. 7. Critical supersaturation for homogeneous nucleation, according to classical theory, and heterogeneous nucleation, against temperature.

several assumed nucleus sizes R_0, and homogeneous nucleation, using the classical theory (Becker and Döring, 1935), are shown against temperature. For the homogeneous process, a supersaturation corresponding to a nucleation rate of $10^6\,m^{-3}\,s^{-1}$ has been used. Classical homogeneous nucleation theory is known to be inadequate in many situations, so the homogeneous nucleation threshold may be incorrect. At $S_r = 65$ and at a temperature of 133°C (the value of T_N for $T_r = 120$°C) either homogeneous nucleation is taking place, the classical theory overpredicting the threshold supersaturation by a factor of about 6 (which is possible but unlikely), or nucleation is heterogeneous, with nuclei of radius about 0.7 nm. Presumably, such nuclei are generated either by chemical reactions in the cavity, or are introduced with the argon replenishment.

As for the transport of sodium onto the roof, a calculation for a pool temperature of 520°C, when the aerosol density is $13.6\,gm^{-3}$, leads to a condensation rate of $0.014\,mg\,m^{-2}\,s^{-1}$, and an aerosol mass transfer rate to the roof of $0.008\,mg\,m^{-2}\,s^{-1}$, mostly by thermophoresis.

6. CONCLUSIONS

The main conclusion of this work is that it seems to be possible to correlate the aerosol properties in a cover gas space using a single value of roof supersaturation for a range of pool temperatures. This supersaturation corresponds to the threshold for rapid nucleation, either homogeneous or heterogeneous using nuclei of a narrow size range. The steady state is maintained by a balance between the rate of nucleation and the rate of droplet removal.

It remains to be seen whether the roof supersaturation of 65 for a roof temperature of 120°C, found to be appropriate in the Himeno–Takahashi experiments, can be used in the analysis of other experiments. If the nucleation is heterogeneous, then the supersaturation threshold depends on the radius of the nuclei, and in other experiments this may change, depending to some extent on the argon replenishment system, or on the sodium purity.

The Himeno–Takahashi experiments also illustrate two mechanisms of particle creation: nucleation for a pool temperature greater than 350°C, and particle injection below this temperature. Injection means the introduction into the cavity of μm size particles onto which sodium condensation can occur. It thus may be considered to be an extreme case of heterogeneous nucleation; the nuclei for this process normally being nm in size. The transition temperature at 350°C corresponds to the lowest pool temperature at which it is possible to generate a threshold supersaturation of 65 at the roof, and hence the lowest pool temperature at which particle nucleation is possible.

Acknowledgement—This work was funded by the U.K. Department of Trade and Industry through AEA Reactor Services.

REFERENCES

Barnett, P. J., Gentry, P. J., Jackson, D. and Tong, D. K. W. (1985) Emissivity measurements of liquid sodium and some sodium contaminated surfaces. *Proceedings of the International Working Group on Fast Reactors Specialist Meeting on Heat and Mass Transfer in the Reactor Cover Gas*, Harwell, 1985, published by the IAEA.

Barrett, J. C. and Clement, C. F. (1985) The effect of sodium aerosols on total heat transfer and temperature in the cover gas space. *Proceedings of the International Working Group on Fast Reactors Specialist Meeting on Heat and Mass Transfer in the Reactor Cover Gas*, Harwell, 1985, published by the IAEA.

Barrett, J. C. and Clement, C. F. (1990) Growth and redistribution in a droplet cloud interacting with radiation. *J. Aerosol Sci.* **21**, 761.

Barrett, J. C., Clement, C. F. and Ford, I. J. (1992) The effect of redistribution on aerosol removal rates. *J. Aerosol Sci.* **23**, 639.

Becker, R. and Döring, W. (1935) *Ann. Physik* **21**, 719.

Clement, C. F. (1985a) Aerosol formation from heat and mass transfer in vapour–gas mixtures. *Proc. Roy. Soc.* **A398**, 307.

Clement, C. F. (1985b) Aerosol growth in the cover gas space. Harwell report TP.1158.

Clement, C. F. (1987) The supersaturation in vapour-gas mixtures condensing into aerosols. Harwell report TP.1223.

Himeno, Y. and Takahashi, J. (1980) Sodium mist behaviour in cover gas space of LMFBR. *J. Nucl. Sci. and Tech.* **17,** 404.

Lifshitz, I. M. and Slyozov, V. V. (1961) The kinetics of precipitation from supersaturated solid solutions. *J. Phys. Chem. Solids* **19,** 35.

McAdams, W. H. (1954) *Heat Transmission,* Chapter 7. McGraw-Hill, New York.

Sinai, Y. L., Ford, I. J., Barrett, J. C. and Clement, C. F. (1993) Prediction of coupled heat and mass transfer in the fast reactor cover gas: the C-GAS code. To appear in *Nuclear Engineering and Design.*

Talbot, L., Cheng, R. K., Schefer, R. W. and Willis, D. R. (1980) Thermophoresis of particles in a heated boundary layer. *J. Fluid Mech.* **101,** 737.

Williams, M. M. R. (1983) Radiant heat transfer through an aerosol suspended in a transparent gas. *IMA J. appl. Maths* **31,** 37.

Williams, M. M. R. (1984) Radiant heat transfer through an aerosol suspended in a transparent gas: addendum. *IMA J. appl. Maths* **33,** 101.

Williams, M. M. R. (1988) A unified theory of aerosol coagulation. *J. Phys. D: Appl. Phys.* **21,** 875.